gas, and transitory heating of pre-existing nebular or interstellar dust. At present, there is a consensus that they formed by transitory heating of "cool" (<1000 K) nebular dust. Possibilities include collisions of small (<1 m) bodies, frictional heating of dust traveling through gas during infall, lightning, energy released by magnetic flares or reconnection of magnetic field lines, and radiative heating resulting from high-velocity outflows during the T-Tauri phase (see later) of the protosun. The leading hypothesis is that most chondrules were produced in shock waves in the solar nebula. Such shock waves could have been produced by accretion shocks, bow shocks from planetesimals, infalling clumps, interactions with passing stars, or spiral density waves. The latter result from uneven distribution of mass in the nebula and resulting gravitational torques. They can be thought of as somewhat analogous to spiral arms of galaxies. Shocks produce heating because gas is accelerated in the shocks more rapidly than dust, so that the dust is heated by gas drag. Numerical modeling by Desch and Connolly (2002) has shown that shock waves can produce the rapid heating and cooling that chondrules apparently experienced. Such shock waves must have been common in the inner solar system because 40% or so of the dust that ultimately formed the asteroids and the terrestrial planets was processed into chondrules. Some chondrules might have formed by other mechanisms: usual features of chondrules in CB chondrites suggest they may be formed in a high-energy collision between planetesimals.

10.3.1.3 Calcium-aluminum inclusions

Ca-Al inclusions or CAIs are submillimeter to centimeter-sized clasts consisting primarily of calcium- and aluminum-rich minerals. They were first described only in 1968 and were at first thought to be restricted to just the CO, CV, and CM chondrites. However, they have now been recognized in essentially all chondrite classes, except CI, although they are rare, and typically very small, in all except the carbonaceous chondrites. The principal minerals are spinel ($MgAl_2O_4$), melilite ($Ca_2Al_2SiO_7$–$Ca_2Mg_2Si_2O_7$), perovskite ($CaTiO_3$), hibonite ($CaAl_{12}O_{19}$), anorthite ($CaAl_2Si_2O_8$), and calcic pyroxene ($CaMg_2Si_2O_6$). Forsteritic olivine is also common in one subtype (forsterite, of course, is not a Ca-Al mineral *per se*, although some forsterites in CAIs are relative rich in the Ca olivine end member, monticellite). Ni-Fe alloys (taenite, kamacite, awaruite) and a wide variety of other minerals may also be present as minor or trace phases.

CAIs have attracted great interest for several reasons. First, they consist of those minerals thermodynamically predicted to condense first as hot gas of solar composition cools. Consistent with this, CAIs are remarkably poor in the more volatile elements (except where they have been altered by secondary processes on parent bodies) and they are rich in refractory trace elements such as Ba, Th, Zr, Hf, Nb, Ta, Y, and the rare earths. They sometimes contain microscopic metallic nuggets, called *fremdlinge,* that consist of metals, such as Re, Os, Re, Pt, Ir, W, and Mo, which condense at temperatures even higher than the Ca-Al minerals. Second, as we shall see in a subsequent section, they are the oldest dated objects in the solar system, pre-dating other chondritic components by several million years.

A number of different types of CAIs have been recognized. The most common type is the so-called *spinel-pyroxene inclusions*, which are typically much smaller than 1 mm in diameter (except in CV3 meteorites) and consist of small spinel grains or clumps of grains enveloped in aluminous diopside, sometimes accompanied by anorthite. *Type A* CAIs are less than 1 mm in diameter (except in CV3 meteorites) and consist primarily of melilite intergrown with hibonite, spinel, perovskite, and noble metal nuggets. Most have a fluffy texture and irregular shape; more rarely they can be spherical and compact. Both the Type A and the spinel-pyroxene inclusions can be more than 1 cm in diameter in CV3 meteorites. *Type B* inclusions are typically larger, up to 1 cm in diameter, more varied in composition, and are restricted to CV3 meteorites. One subtype consists of coarse-grained melilite, calcic pyroxene, anorthite, and spinel. Another subtype consists of forsterite, melilite, calcic pyroxene, and spinel. *Type C* CAIs, which are rare, consist mostly of spinel, calcic pyroxene, and anorthite. A fifth type, the so-called *hibonite-rich CAIs*, consist of hibonite, sometimes

accompanied by spinel and perovskite. A sixth type, the *hibonite-silicate spherules*, consist of hibonite intergrown with aluminous pyroxene and perovskite embedded in glass of aluminous pyroxene composition. All types of CAIs are typically surrounded by an accretionary rim several tens of μm thick, typically consisting of the same minerals as are present in the interior, that appears to have resulted from high-temperature gas–solid or gas–melt interaction.

Although CAIs as a whole have compositions that approximate that of the highest temperature condensate of a gas of solar composition, their compositions do not match a condensation trend exactly. Furthermore, the textures of most types of CAIs indicate that they have experienced complex histories, including episodes of melting, evaporation, reaction with nebular gas and finally aqueous alteration and/or metamorphism on parent bodies (Grossman, 2010). However, some CAIs, notably the fluffy Type A inclusions, do have compositions and textures suggesting they are indeed high-temperature condensates of nebular gas. It is possible that many other CAIs began as such condensates and they experienced subsequent episodes of transient high temperatures. Other CAIs may have formed as evaporative residues. Regardless of the details, CAIs provide evidence that some nebular dust experienced transient heating events with temperatures reaching 1700 K. This is much hotter than the nebula should have ever been at the position of the asteroid belt. For this and other reasons, there is an emerging consensus that CAIs formed close to the Sun and were subsequently cycled back out into the deeper nebula, perhaps by "X-winds", which we will discuss later in the chapter.

10.3.1.4 Amoeboidal olivine aggregates

Amoeboidal olivine aggregates (AOAs) are, as their name implies, aggregates of anhedral forsteritic olivine with lesser amounts of Fe-Ni metal, spinel, aluminous diopside, and rare anorthite and melilite. They are fine-grained (5–20 μm) and the aggregates have dimensions similar to those of chondrules in the same meteorite. Some contain melted CAIs. In some cases, the olivine is partially replaced by enstatite. Some have igneous textures, suggesting they have been partially melted. AOAs most likely represent aggregates of grains that condensed from nebular gas at high temperature. They may well have formed in the same environment, albeit at lower temperature, as CAIs.

10.3.1.5 The chondrite matrix

The matrix of chondrites is dark, FeO- and volatile-rich material that is very fine-grained (typical grain size is about 1 μm). It can be quite heterogeneous, even on a 10 μm scale. It also varies between meteorite classes, with an order of magnitude variation in Mg/Si, Al/Si and Na/Si. The primary constituents appear to be Fe- and Ca-poor pyroxene and olivine and amorphous material, but magnetite, Fe-metal, and a wide variety of silicates, sulfides, carbonates, and other minerals are also present. In the most volatile-rich meteorites the olivine and pyroxene have been altered to serpentine and chlorite; in the carbonaceous chondrites, carbonaceous material is present in substantial quantities. On the whole, the composition of the matrix is complementary to that of the chondrules: whereas the latter are depleted in Fe and volatiles, the former are enriched in them. Very significantly, the matrix includes grains of SiC, graphite, diamond and other phases of anomalous isotopic composition. These "presolar grains" are of great significance and we will discuss these isotopic variations in greater detail in a subsequent section.

10.3.2 Differentiated meteorites

The differentiated meteorites are products of melting on asteroid parent bodies. They are igneous rocks with igneous textures, although in some cases, brecciation may be the dominant texture.

10.3.2.1 Achondrites

While all the chondrites seem reasonably closely related, the achondrites are a more varied group. The *Acapulcoites*, *Lodranites*, *Winonaites*, and *Urelites* form a group called the *primitive achondrites* because they resemble chondrites in composition and mineralogy. Beyond that they are quite diverse. Meteorites of the first three groups are

extremely rare. They represent chondritic material that has experienced extreme metamorphism and low-degree partial melting. In a few cases, relict chondrules have been identified, providing further evidence of their primitive nature. *Urelites*, which are both more common and more diverse than the other primitive achondrites, consist of olivine, pyroxene, and a few metal grains plus a percent or so carbon, present as graphite and diamond, the latter a product of shock metamorphism produced by impacts. Their origin is problematic; it is possible they have several origins. Some are partial melting residues like other primitive achondrites; others appear to be highly fractionated igneous rocks. *Brachinites* are also sometimes included in the primitive achondrites.

Upon heating, chondritic material will first form a metal-sulfide melt, which is much denser than the mainly silicate residual solid. This metal will drain out of the matrix and ultimately form a core at the center of the body. Upon further heating, a silicate partial melt will form, into which the more incompatible elements will partition. Thus primitive achondrites are variously depleted in metal and incompatible elements relative to chondrites.

Figure 10.16 illustrates the compositional relationship between the various achondrite groups. Primitive achondrites tend to have Mn/Mg ratios similar to those of chondrites, while the remaining achondrites have superchondritic Mn/Mg ratios and Fe/Mg ratios higher than primitive achondrites. This, as well as their texture and mineralogy, indicates that those remaining achondrite groups originated through igneous processes. During partial melting of chondritic material, these three elements partition into the melt in the order Mn > Fe > Mg. Subsequent fractional crystallization increases the Fe/Mg ratio, but has little further effect on the Mn/Fe ratio.

Diogenites are Ca-poor and consist principally of hypersthene (orthopyroxene), which is accompanied by minor amounts of olivine and plagioclase. They are coarse-grained and their texture suggests they formed as cumulates in a magma chamber. The Ca-rich achondrites include the *eucrites* and *howardites*. The eucrites resemble lunar and, to a lesser extent, terrestrial basalts, and are also called *basaltic achondrites*, and like terrestrial

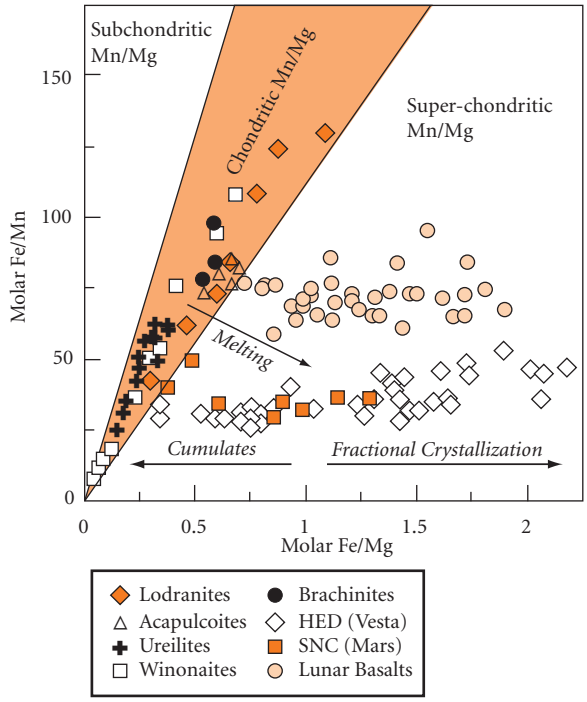

Figure 10.16 Variation in Fe/Mn and Fe/Mg ratios in achondrites and lunar basalts. Primitive achondrites are variably depleted in Fe, but have Mn/Mg ratios similar to chondrites. The HED and SNC chondrites, like lunar basalts, have superchondritic Mn/Mg ratios and higher Fe/Mg ratios than primitive achondrites as a consequence of their igneous origin. Data from Goodrich and Delaney (2000).

basalts they consist primarily of plagioclase and pyroxene. The howardites are extremely brecciated, and are a heterogeneous mixture of eucrite and diogenite material. They also contain clasts of carbonaceous chondritic material, other xenolithic inclusions, and impact melt clasts. Their brecciated character suggests they were part of the regolith, or surface, of their asteroid parent body. The howardites, eucrites, and diogenites for a group, collectively called the HED meteorites, comprise about 6% of all falls. They have long been believed to come from the asteroid *4 Vesta* (Figure 10.17). This association was confirmed by data obtained by NASA's Dawn spacecraft's visible and infrared spectrometer (De Sanctis *et al.*, 2012). Dawn orbited Vesta

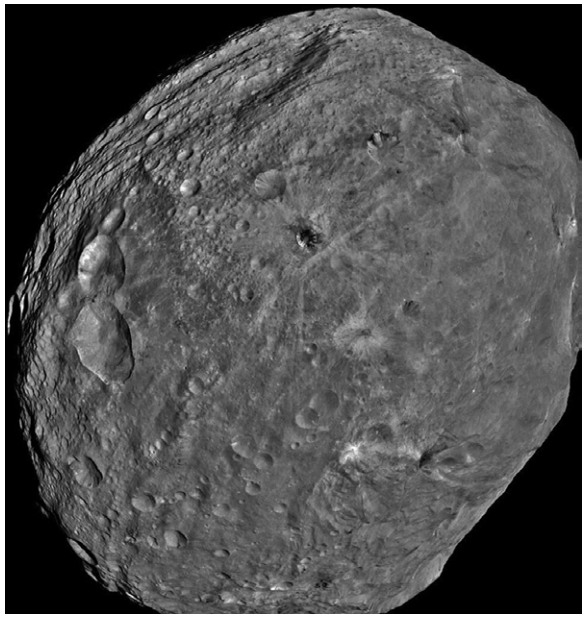

Figure 10.17 Photograph of the asteroid 4 Vesta taken by the NASA Dawn spacecraft in 2011. Vesta, the second most massive asteroid, has a semi-major orbital axis of 2.4 AU, a mean diameter of 500 km and a mean density of 3420 kg/m^3. It is believed to be the parent body of the HED meteorites. Image: NASA.

for 13 months in 2011 and 2012 before heading for *1 Ceres*.

Two final groups are the *angrites* and the *aubrites*. The angrites (of which there are only four specimens, the name of the class being derived from *Angra dos Reis*) consist mostly of Al-Ti augite (Ca-rich pyroxene). They are strongly silica-undersaturated, contain minerals characteristic of alkali basalts such as nepheline, and are strongly depleted in moderately volatile elements. The compositions suggest formation through partial melting under oxidizing conditions, followed by complex igneous differentiation. In contrast, the aubrites are highly reduced and consist primarily of enstatite. They resemble enstatite chondrites, but they do not contain chondrules and they are poorer in metal and sulfide. It seems nonetheless highly likely that they formed from enstatite chondrite parent material.

A unique group of achondrites, the *SNC* meteorites (the name is derived from type meteorites *Sherogotty, Nakla,* and *Chassigny*)

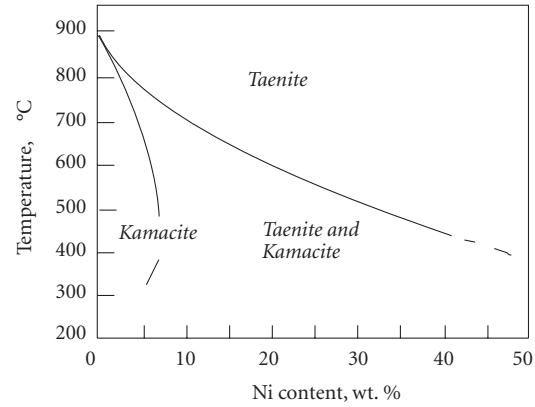

Figure 10.18 Phase diagram for iron-nickel alloy. Wasson (1974). With kind permission of Springer Science+Business Media.

generally have much younger formation ages (0.15–1.5 Ga) than virtually all other meteorites. This, and certain features of their bulk compositions and trapped noble gases, has led to the interpretation that these meteorites come from Mars, having been ejected by an impact event on that planet. This interpretation, initially controversial, is now the consensus view. There are 92 distinct specimens of this class (excluding pairing, that is, ones that are clearly pieces of the same rock). Finally, there are 25 meteorites of lunar origin. A handful of achondrites are unique and cannot be assigned to any class.

10.3.2.2 Irons

Iron meteorites were originally classified based largely on phase and textural relationships. Compositionally, they all consist primarily of Fe-Ni alloys with lesser amounts of (mainly Fe-Ni) sulfides. Octahedral taenite, one of the Fe-Ni alloys, is the stable Fe-Ni metal phase at T > 900°C (Figure 10.18). At lower temperature, kamacite, a Ni-poor Fe-Ni alloy, exsolves on the crystal faces of the octahedron. If the Ni content falls below 6%, all the metal converts to kamacite at lower temperature. Thus the phases and textures of iron meteorites are related to their composition and cooling history. Iron meteorites consisting only of kamacite are named *hexahedrites*. If Ni exceeds 6%, some taenite persists and the overall pattern is octahedral (= *octahedrites*), producing what is known as a *Widmanstätten* pattern. At low Ni contents, kamacite domi-

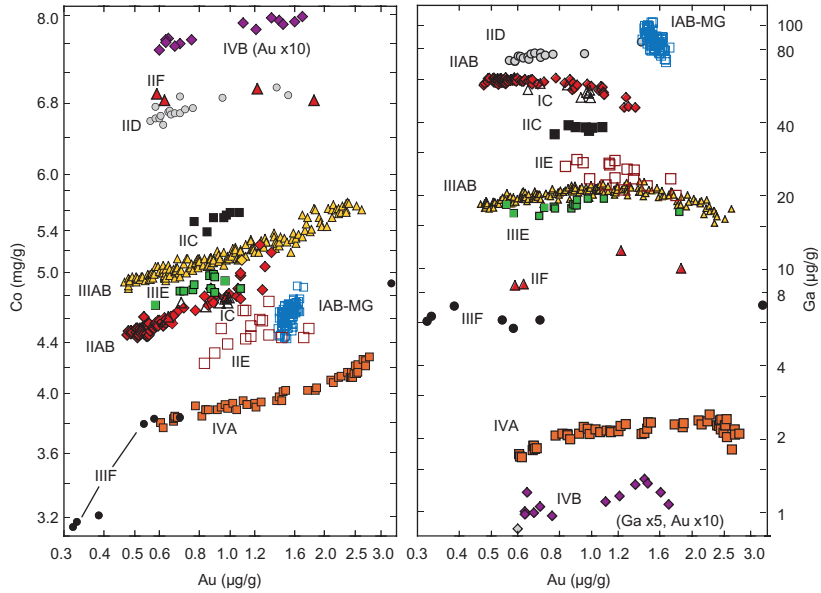

Figure 10.19 Co-Au and Ga-Au plots illustrating the compositional distinctions and variations in groups of iron meteorites. IAB-MG refers to the "main group" of IAB irons, while other subgroups of the IAB irons show more scatter. Reproduced with permission of John T. Wasson.

nates and forms large crystals (*coarse octahedrites*). At higher Ni, kamacite and crystal size diminish (*fine and medium octahedrites*). *Ataxites* are Ni-rich (>14%) iron meteorites consisting of a fine-grained intergrowth of kamacite and taenite. The 20% or so of irons with silicate inclusions form a separate class.

Wasson (1985) subsequently reclassified the irons based on composition, specifically on Ga-Ni and Ge-Ni abundances. The classes were named I–IV, based on decreasing Ga and Ge. Subgroups within these classes were named A, B, and so on. Wasson and Kallemeyn (2002) and Wasson (2011) subsequently found that gold concentrations delineated these classes better than did nickel concentrations. Figure 10.19 illustrates the classification and chemical variation among iron meteorites based on the relationships between gold, cobalt, and gallium concentrations.

The chemical variations within individual subclasses of irons are consistent with those produced by fractional crystallization of metal liquid. The clear implication is that all irons from an individual subclass come from a single parent body. Perhaps some 60 parent bodies are represented by the suite of analyzed irons. There is a general consensus that iron meteorites, with a few notable exceptions, represent the cores of asteroids or *planetesimals*. Cooling rates, estimated from textures and diffusion profiles, are typically in the range of a few tens of degrees per million years. This slow cooling indicates the irons formed in the interior of bodies with diameters in the range of a few tens to a few hundreds of kilometers. A few classes of irons, most notably the IAB, may represent impact melts rather than segregated cores. Based on the oxygen isotope composition of their silicate inclusions, Wasson and Kallemeyn (2002) speculated that the main group of IAB irons represent a single melt body formed by an impact on a carbonaceous chondrite asteroid, and that the elemental trends were formed by crystal separation during downward flow in the asteroid.

10.3.2.3 Stony-irons

The main classes of stony-irons are the *pallasites* and the *mesosiderites*. Pallasites consist of a network of Fe-Ni metal with nodules of olivine. They probably formed at the interface between molten metal and molten silicate bodies, with olivine sinking to the bottom of the silicate magma. Mesosiderites consist of an odd pairing of metal and silicate. The silicate portion is very similar to diogenites – brecciated pyroxene and plagioclase – and a

genetic relationship is confirmed by oxygen isotopes (discussed later). The metal fraction seems closely related to IIIAB irons. It is possible they formed as the result of a collision of two differentiated asteroids, with the liquid core of one asteroid mixing with the regolith of the other.

10.4 TIME AND THE ISOTOPIC COMPOSITION OF THE SOLAR SYSTEM

10.4.1 Meteorite ages

10.4.1.1 Conventional methods

Meteorite ages are generally taken to be the age of solar system. Before we discuss meteorite ages in detail, we need to consider the question of precisely what event is being dated by radiometric chronometers. In Chapter 8, we found that radioactive clocks record the last time the isotope ratio of the daughter element (e.g., $^{87}Sr/^{86}Sr$) was homogenized. This is usually some thermal event. In the context of what we know of early solar system history, the event dated might be (1) the point when solid particles were removed from a homogenous solar nebula, (2) thermal metamorphism in meteorite parent bodies, or (3) crystallization (in the case of chondrules and achondrites), or (4) impact metamorphism of meteorites or their parent bodies. In some cases, the nature of the event being dated is unclear.

The most precise ages of meteorites have been obtained using the U-Pb chronometer (Figure 10.20). Advances in analytical techniques have remarkably improved precision over the last decade or so, to the point that ages with uncertainties of only a few 100,000 years can be obtained. However, some of the issues that traditionally plague geochronology come into focus, including lack of complete initial isotopic homogeneity and deviations from closed system behavior. In addition, new issues arise, including uncertainties in half-lives of the parents and uncertainty in, as well as variation of, the $^{238}U/^{235}U$ ratio (Amelin *et al.*, 2009). Progress is being made in resolving these issues, but further research remains necessary.

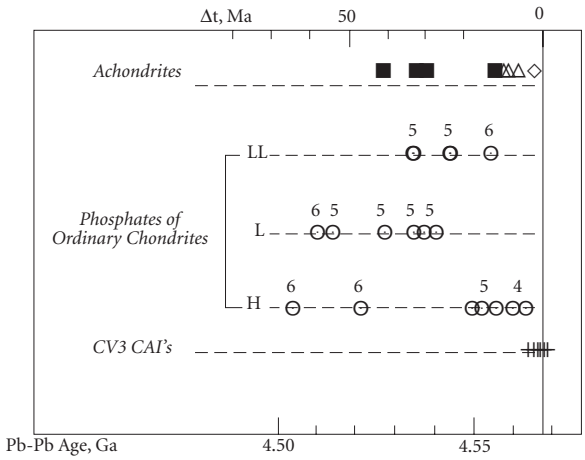

Figure 10.20 High precision Pb-Pb ages of Allende CAIs, ordinary chondrites, and achondrites. Allegre (2001). By permission of the Royal Society.

The oldest Pb-Pb ages come from CAIs, in part because CAIs are rich in refractory elements like U and depleted in volatile elements like Pb. At present, the oldest high-precision date is 4568.67 ± 0.17 Ma for a CAI from the CV3 meteorite *NWA2364** calculated using the "canonical" $^{238}U/^{235}U$ ratio of 137.88 (Bouvier and Wadhwa, 2010). This age decreases to 4568.22 ± 0.17 Ma if a value of 137.84 is used for that ratio. Bouvier and Wadhwa (2010) speculated that the $^{238}U/^{235}U$ of the CAI might be as low as 137.81, which would make the age 0.3 Ma younger. The next oldest age is a CAI from *Allende*, also CV3 meteorite, whose age, calculated using the canonical $^{238}U/^{235}U$ value, is 4567.59 ± 0.11 Ma (Bouvier *et al.*, 2007). Less precise ages ranging from 4567.4 to 4568.6 have been reported for other *Allende* inclusions. Amelin *et al.* (2009) reported a high-precision Pb-Pb age of 4567.11 ± 0.16 Ma for a CAI from the CV3 meteorite *Efremovka*. The accuracy of these dates has, however, been thrown into question by Brennecka *et al.*'s (2010) discovery of variable $^{238}U/^{235}U$ ratios in CAIs from Allende, which range from 137.409 ± 0.039 to 137.885 ± 0.009, compared with the "canonical" value of 137.88. Brennecka *et al.* (2010) concluded that the

* NWA stands for Northwest Africa. This is one of many meteorites found in the Sahara desert over the last couple of decades.

cause of the variability was decay of ^{247}Cm, which decays to ^{235}U with a half-life of 13.6 Ma. Amelin *et al.* (2010) calculated an age for one *Allende* CAI using the ^{238}U/^{235}U measured in that CAI (137.876) and obtained an age of 4567.18 ± 0.50 Ma. Because the ^{238}U/^{235}U is very close to the "canonical" value, this age falls well within error of Pb-Pb ages of other CV3 CAIs. Bouvier and Wadhwa (2010) speculated that the slightly older age of *NWA2364* inclusions compared with those of *Allende* and *Efremovka* might reflect aqueous alteration of the latter after incorporation into the CV3 parent body. Chondrules in carbonaceous chondrites have slightly younger Pb-Pb ages than the CAIs, 4562.7 ± 0.5 for *Gujba* (CB3) to 4565.5 ± 0.5 Ga for *Allende*. The ages assume the canonical ^{238}U/^{235}U value. Amelin *et al.* (2010) found that the *Allende* whole rock and chondrules had a low ^{238}U/^{235}U, 137.747 ± 0.017, which implies earlier reported ages of the chondrules were too old by about 1.4 Ma.

Phosphates also have high U/Pb ratios and these were analyzed by Göpel *et al.* (1994) to obtain high-precision ages of a variety of equilibrated (i.e., petrologic classes 4–6) ordinary chondrites, whose ages range from 4.563 to 4.502 Ga. The phosphates are thought to have formed during metamorphism, thus these ages represent the age of metamorphism of these meteorites. The oldest of these meteorites was H4 chondrite *Ste. Marguerite*. Bouvier *et al.* (2007) subsequently reported a Pb-Pb isochron age of 4562.7 Ma, in excellent agreement with the age determined by Göpel *et al.* (1994). The age of CAIs from CV3 meteorites thus seem 3 Ma older than the oldest precise ages obtained on ordinary chondrites. No attempt has been made at high-precision dating of CI chondrites, as they are too fine-grained to separate phases.

Among achondrites, the chronology of the angites is perhaps best documented. The oldest high-precision Pb-Pb age is 4564.42 ± 0.12 Ma for the angrite *D'Orbigny* (Amelin, 2008). This age was calculated assuming ^{238}U/^{235}U = 137.88. Using the measured ^{238}U/^{235}U for this meteorite of 137.778, the age is reduced to 4563.36 ± 0.34 (Bouvier *et al.*, 2011). *Angra dos Reis* has a Pb-Pb age of 4557.65 ± 0.13 Ma, and *Lewis Cliff 86010*, a coarse-grained "plutonic" angrite, has an age of 4558.55 ± 0.15 Ma. Thus differentiation, cooling and crystallization of the angrite parent body apparently lasted some 6 million years. Wadhwa *et al.* (2009) reported an age of 4566.5 ± 0.2 Ma for unusual basaltic achondrite, *Asuka 881394*. Bouvier *et al.* (2011) determined an age of 4562.89 ± 0.59 Ma for another unusual basaltic achondrite, *NWA2976*. *Ibitira*, a unique unbrecciated eucrite, has an age of 4556 ± 6 Ma. Perhaps surprisingly, these ages are similar to those of chondrites. This suggests that the parent body of these objects formed, melted, and differentiated, and the outer parts crystallized, within a very short time interval. Not all achondrites are quite so old, however. A few other high-precision ages (those with quoted errors of less than 10 Ma) are available and they range from this value down to 4.529 ± 0.005 Ga for *Nuevo Laredo* and 4.510 ± 0.004 Ga for *Bouvante*. Thus the total range of the few high-precision ages in achondrites is about 50 million years. Iron meteorites appear to be similarly old. Smoliar *et al.* (1996) reported Re-Os ages of 4558 ± 12 and 4537 ± 8 Ma for IIIA and IIA irons, respectively; ages of other iron groups range from 4506 to 4569 Ma, but are of lower precision and are not significantly different from the IIIA and IIA ages.

K-Ar ages are often much younger. This probably reflects Ar outgassing as a result of collisions, and the ages probably date impact metamorphism.

As Figure 10.20 shows, there is little relationship between meteorite class and age. H chondrites do seem a bit older than other ordinary chondrites, and Göpel *et al.* (1994) did find an inverse correlation between petrologic type and age (the least metamorphosed are oldest), but this does not appear to be true of chondrites in general. Furthermore, there appears to be little difference in age between chondrites and achondrites. The present state of conventional meteorite chronology may be summarized by saying that it appears the meteorite parent bodies formed at around 4.567 ± 0.001 Ga, and there is some evidence that high-temperature inclusions and chondrules in carbonaceous chondrites may have formed a few million years earlier than other material. At least some parent bodies remained hot enough to allow metamorphism to continue for some 30 Ma after their formation. Resolving events on a finer time-scale than

this has proved difficult using conventional techniques. There are, however, other techniques that help to resolve events in early solar system history, and we now turn to these.

10.4.1.2 Initial ratios

The reference "initial" $^{87}Sr/^{86}Sr$ of the solar system is taken as 0.69897 ± 3, based on the work of Papanastassiou and Wasserburg (1969) on basaltic achondrites (BABI: basaltic achondrite best initial). Basaltic achondrites were chosen since they have low Rb/Sr and hence the initial ratio (but not the age) is well constrained in an isochron. Subsequent high-precision analyses of individual achondrites yield identical results (earlier-reported low values from *Angra Dos Reis* have subsequently been shown to be in error). CAIs and Rb-poor chondrules from *Allende* have an even lower initial ratio – 0.69877 ± 3 – consistent with the idea that these formed slightly earlier than the meteorite parent bodies.

The initial $^{143}Nd/^{144}Nd$ ratio of the solar system is taken as 0.506609 ± 8 (normalized to $^{146}Nd/^{144}Nd = 0.72190$) based on the work on chondrites of Jacobsen and Wasserburg (1980). Achondrites seem to have slightly higher initial ratios, suggesting they formed a bit later.

The initial isotopic composition of Pb is taken from the work of Tatsumoto *et al.* (1973) on troilite from the Canyon Diablo iron meteorite as: $^{206}Pb/^{204}Pb$, 9.307; $^{207}Pb/^{204}Pb$, 10.294; $^{208}Pb/^{204}Pb$, 29.476. These values agree with the best initial values determined from chondrites, including *Allende* chondrules. Subsequent work by Chen and Wasserburg (1983) confirmed these results: 9.3066, 10.293, and 29.475 respectively.

10.4.1.3 Extinct radionuclides

There is abundant and compelling evidence that certain short-lived nuclides once existed in meteorites. This evidence consists of anomalously high abundances of the daughter nuclides in certain meteorites, and fractions of meteorites that correlate with the abundance of the parent element. The first of these to be discovered was the ^{129}I–^{129}Xe decay (Reynolds, 1960). Since then, 18 other *extinct radionuclides* have been discovered. The most significant of these are listed in Table 10.4; a full list can be found in Dauphas and Chaussidon (2011). These provide evidence of nucleosynthesis occurring shortly before the solar system formed. To understand why, consider the example of ^{129}I. It decays to ^{129}Xe with a half-life of 16 Ma. Hence 16 Ma after they were created, only 50% of the original atoms of ^{129}I would remain. After two half-lives or 32 Ma, only 25% would remain, after four half-lives or 64 Ma only 6.125% of the original ^{129}I would remain, and so on. After 10 half lives, or 160 Ma, only $½^{10}$ (0.1%) of the original amount would remain. Anomalously high abundance of ^{129}Xe relative to other Xe isotopes that correlate with iodine concentration in a meteorite indicates some ^{129}I was present when the meteorite, or its

Table 10.4 Short-lived radionuclides in the early solar system.

Radio-nuclide	Half-life Ma	Decay	Daughter	Abundance ratio
^{10}Be	1.5	β	^{10}B	$^{10}Be/^{9}Be \sim 7.5 \times 10^{-4}$
^{26}Al	0.73	β	^{26}Mg	$^{26}Al/^{27}Al = 5.2 \times 10^{-5}$
^{36}Cl	0.301	β	$^{36}Ar/^{36}S$	$^{36}Cl/^{35}Cl \sim 17 \times 10^{-6}$
^{41}Ca	0.15	β	^{41}K	$^{41}Ca/^{40}Ca \sim 1.4 \times 10^{-8}$
^{53}Mn	3.7	β	^{53}Cr	$^{53}Mn/^{55}Mn = 6.3 \times 10^{-6}$
^{60}Fe	1.5	β	^{60}Ni	$^{60}Fe/^{56}Fe \sim 5.8 \times 10^{-8}$
^{107}Pd	9.4	β	^{107}Ag	$^{107}Pd/^{108}Pd \sim 5.9 \times 10^{-4}$
^{129}I	16	β	^{129}Xe	$^{129}I/^{127}I \sim 1.2 \times 10^{-4}$
^{146}Sm	68	α	^{142}Nd	$^{146}Sm/^{144}Sm = 0.0094$
^{182}Hf	8.9	β	^{182}W	$^{182}Hf/^{180}Hf = 9.7 \times 10^{-5}$
^{244}Pu	82	α, SF	Xe	$^{244}Pu/^{238}U \sim 0.001$
^{247}Cm	15.6	α, SF	^{235}U	$^{247}Cm/^{235}U \sim 6 \times 10^{-5}$

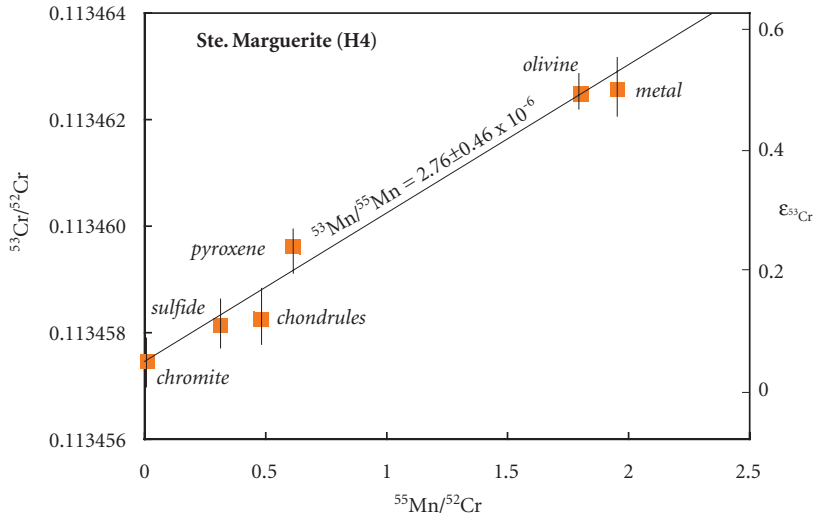

Figure 10.21 Correlation of the $^{53}Cr/^{52}Cr$ ratio with $^{55}Mn/^{52}Cr$ ratio in inclusions from the ordinary chondrite *Ste. Marguerite* (H4). Trinquier *et al.* (2008). With permission from Elsevier.

parent body, formed. From this we can conclude that ^{129}I had been synthesized not more than roughly 10^8 years before the meteorite formed. This time constraint is further reduced by the identification of radiogenic ^{26}Mg, produced by the decay of ^{26}Al. That ^{26}Al is the source of the ^{26}Mg is evidenced by the correlation between ^{26}Mg and the Al/Mg ratio. The half-life of ^{26}Al is 0.73 Ma and the production ratio for $^{26}Al/^{27}Al$ in red giants is thought to be around 10^{-3} to 10^{-4}. The $^{26}Al/^{27}Al$ initial ratios in CAIs of 5×10^{-5} indicates that nucleosynthesis occurred no more than a few million years before formation of these CAIs.

These short-lived "fossil" radionuclides also provide a means of relative dating of meteorites and other bodies, because the abundance of the extinct radionuclide at the time an object formed can be deduced. Consider Figure 10.21 where $^{53}Cr/^{52}Cr$ in inclusions from *Allende* are plotted as a function of the $^{55}Mn/^{52}Cr$. Provided that (1) all inclusions formed at the same time, (2) all remained closed to Mn and Cr since that time, and (3) ^{53}Mn was present when they formed and has since fully decayed, we can derive the following equation from the fundamental equation of radioactive decay:

$$\left(\frac{^{53}Cr}{^{52}Cr}\right) = \left(\frac{^{53}Cr}{^{52}Cr}\right)_0 + \left(\frac{^{53}Mn}{^{55}Mn}\right)_0 \left(\frac{^{55}Mn}{^{52}Cr}\right) \quad (10.1)$$

where, as usual, the subscript nought refers to the initial ratio. On a plot of $^{53}Cr/^{52}Cr$ versus $^{55}Mn/^{52}Cr$ such as Figure 10.21, this is the equation of a line with a slope equal to the initial $^{53}Mn/^{55}Mn$ ratio, in this case 2.76×10^{-6} (note that the right-hand scale expresses the $^{53}Cr/^{52}Cr$ ratio in the epsilon notation introduced in Chapter 8, or deviations in parts per thousand from a terrestrial standard, whose value is 0.1134569).

As time passes, the abundance of the radioactive nuclide will decrease, so that the initial ratio determined in diagrams such as Figure 10.21 will be lower for younger objects. This is illustrated in Figure 10.22, which compares ^{26}Al-^{26}Mg systematics in a CAI from the CV3 meteorite *NWA2364* to those in a younger object, the eucrite *Asuka 881394*. The difference in initial $^{26}Al/^{27}Al$ indicates the latter object is some 4 million years younger than the former.

Extinct radionuclides can thus be used to establish a relative time-scale of events in the early solar system. A number of factors, however, hinder this process. First, it is possible that these recently synthesized radionuclides might not have been uniformly distributed through the solar nebula. Indeed, as we shall see in a subsequent section, there is evidence of isotopic heterogeneity on the very fine scale of the matrix material of carbonaceous chondrites. Second, isotopic heterogeneity

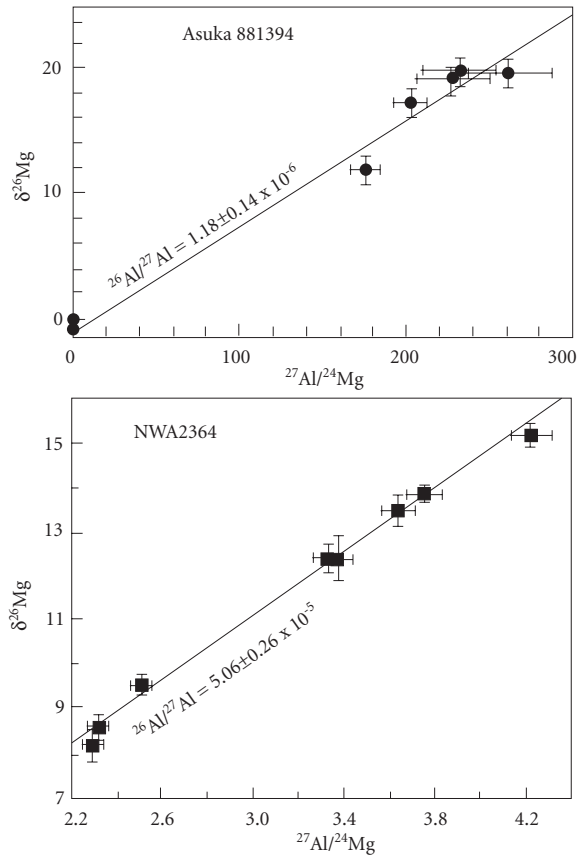

Figure 10.22 Comparison of Al-Mg isotope systematics for two different meteorites. The lower diagram shows minerals separated from a CAI in CV3 *NWA2364*, one of the oldest objects in the solar system (data from Bouvier and Wadhwa, 2010). The upper diagram shows plagioclase and pyroxene separates from the eucrite *Asuka 881394* (data from Nyquist *et al.*, 2003). The latter has an initial $^{27}Al/^{26}Al$ more than 40 times lower than *NWA2364*, implying it is some 4 million years younger.

unrelated to decay of extinct radionuclides might be present in the daughter elements. Indeed, there is some evidence for this in the case of Cr, but a correction can be made by measuring an additional Cr isotope, ^{54}Cr. In the case of a light element such as Mg, mass fractionation arising from chemical or physical processes might affect the $^{26}Mg/^{24}Mg$. This too can be corrected by measuring ^{25}Mg, provided the fractionation was mass-dependent. Finally, cosmic ray spallation reactions have been demonstrated in meteorites, and these can affect some of the elements of interest, but again, corrections for these effects can generally be made. In addition, there are, of course, the same issues with conventional radiogenic isotopic geochronology, such as open system behavior.

Provided these can be overcome, an absolute chronology can be established by calibrating relative ages determined from extinct radionuclides with high precision Pb-Pb ages. For the earliest objects, the short-lived nuclides ^{53}Mn and ^{26}Al have proved most useful. Figure 10.23 illustrates such a time-scale, anchored on objects dated by both Pb-Pb and ^{26}Al or ^{53}Mn. The chronology begins with the CAI from *NWA2364*. Objects such as *Lewis Hills 86010*, *St. Marguerite*, and *D'Orbigny* provide other anchors. Objects such as *Orgueil*, which has not been dated by conventional radiometric methods, can be placed on the time-scale based on their apparent initial $^{26}Al/^{27}Al$ or $^{53}Mn/^{55}Mn$ ratios.

Ages, both conventional radiometric ages and those based on extinct radionuclides, can represent different things. In the case of CAIs, their age might either represent the formation or time of aqueous alteration of the parent body. For the LL3 chondrules, this age may well represent the formation age, but some evidence suggests the chondrule event lasted for as much as 2 million years, so all chondrules need not have the same age. In other cases, such as *Ste. Marguerite*, the age may represent the age of metamorphism. In others, such as the HED parent body, it represents melting and differentiation. The angrites show a range of ages. *D'Orbigny* is a fine-grained igneous rock that probably formed near the surface of the angite parent body, which would have cooled quickly. *Lewis Cliff 86010* is a coarse-grained rock from the interior of the angrite parent body that would have cooled more slowly.

As mentioned, the extinct radionuclides also provide evidence of one or more nucleosynthetic events shortly before, or perhaps even during, the formation of the solar system. ^{41}Ca, which decays to ^{41}K with a half-life of 150,000 yrs, provides perhaps the most stringent constraint of the time of nucleosynthesis. Extinct ^{41}Ca has been identified in CAIs from several CV3 and CM2 meteorites, which had an apparent $^{41}Ca/^{40}Ca$ ratio of 1.4×10^{-8} when they formed. Isotopic variations of Ag

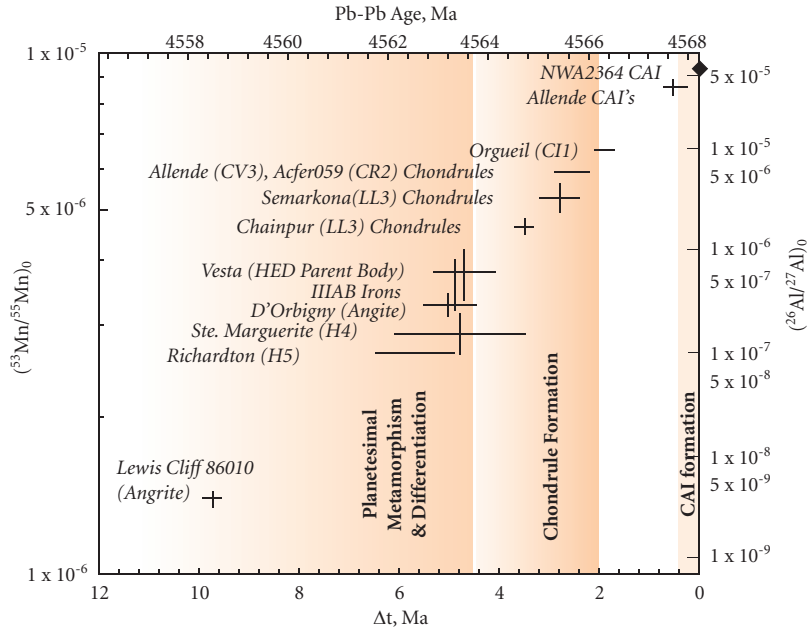

Figure 10.23 Time-scale of events in the early solar system based on calibrating ^{53}Mn and ^{26}Al extinct radionuclide chronology to Pb-Pb ages. Data from Trinquier *et al.* (2008), Nyquist *et al.* (2009) and Bouvier and Wadhwa (2010).

resulting from the decay of ^{107}Pd (half-life 6.5 Ma) in iron meteorites indicate core formation in meteorite parent bodies began, and was largely complete, within about 15 Ma of the nucleosynthesis. We will see at the end of this chapter that the ^{182}Hf-^{182}W pair provides important constraints on timing of formation of the Earth's core.

Exactly how these nuclides were synthesized is somewhat debated. As we saw earlier in this chapter, heavy elements are synthesized mainly in red giant stars and supernovae. On a galactic scale, red giants and supernovae will be continually injecting newly synthesized elements into the interstellar medium. Those nuclides that are unstable will steadily decay away. These two competing processes will result in steady-state abundance of these nuclides in the interstellar medium. The abundances of ^{107}Pd, ^{129}I, ^{146}Sm, and ^{182}Hf listed in Table 10.4 roughly match the expected steady-state galactic abundances and hence do not require a specific synthesis event. However, the abundances of ^{10}Be, ^{26}Al, ^{36}Cl, and ^{41}Ca in the early solar system require synthesis of these nuclides at the time, or just before, the solar system formed.

The conventional view is that these nuclides were synthesized in a red giant and/or a supernova in the region where the solar system formed just shortly before its formation. Some of these elements, such as ^{26}Al, are most efficiently synthesized in red giants; others, such as ^{60}Fe, are most efficiently synthesized in supernovae. Thus most models invoke both environments, which may or may not have been the same star at different times. Indeed, one popular hypothesis is that the formation of the solar system was actually triggered by a supernova shock wave. Boss and Vanhala (2001) provide a good discussion of this view.

Evidence of the existence of ^{10}Be in some CAIs has led to an alternative hypothesis, namely that many of the short-lived extinct radionuclides were produced by spallation within the solar system as it was forming. As we have seen, Be is not synthesized in stars, hence the presence of ^{10}Be in CAIs and other primitive chondritic components is problematic for the red giant/supernova injection hypothesis. Another key observation is that young protostars emit X-rays. X-rays are produced by accelerating charged particles. Hence some have suggested that near the surface of

the accreting protostar, magnetic reconnection events could produce flares that accelerate ions up to very high energies – essentially creating cosmic rays (e.g., Russell *et al.*, 2001). Spallation would occur when the accelerated particles encounter dust grains – the CAIs – that happen to be close to the forming Sun (within 0.1 AU). According to this theory, some of these irradiated CAIs would have been carried back out to the vicinity of the asteroid belt by the energetic "X-winds" that are associated with these protostars.

Most workers now agree that ^{10}Be was synthesized entirely by spallation. Spallation may well have been responsible for some fraction of the ^{26}Al, ^{36}Cl, and ^{41}Ca, and perhaps some of the ^{53}Mn as well. However, it cannot account for the ^{60}Fe and probably cannot account for all of the ^{26}Al, ^{36}Cl, ^{41}Ca, and ^{53}Mn. Huss *et al.* (2009) concluded that intermediate-mass *asymptotic giant branch* (AGB) stars (a variety of red giant) and supernovae of stars with precursor masses in the range of ~20 to ~60 solar masses are the most likely sources.

10.4.2 Cosmic ray exposure ages and meteorite parent-bodies

As we saw in Chapter 8, cosmic rays colliding with matter in meteorites and planetary bodies produce new nuclides through spallation. The cosmic rays only penetrate to a limited depth (of the order of a meter or less: there is no cutoff, the flux falls off exponentially), so that only small bodies or the surfaces of larger bodies are exposed to cosmic rays. The rate of production of nuclides by cosmic ray bombardment can be estimated from experimental physics if the cosmic ray flux is known. Thus, assuming a more or less constant cosmic ray flux, the length of time an object has been exposed to cosmic rays, the "exposure age", can be calculated from the amounts of cosmogenic nuclides. Exposure ages are only accurate to within about a factor of 2, due to all the assumptions that are required in estimating the rate of production of nuclides. Exposure ages for chondrites are shown in Figure 10.24; exposure ages for irons were shown in Figure 8.26. As can be seen, the ages for chondrites are considerably less than formation ages. From this we may conclude that meteorites became small bodies accessible to cosmic rays only comparatively recently. Before that, they must have been stored in larger parent bodies where they would have been protected from cosmic ray bombardment. Apparently, meteorites are continually produced by collisions of these larger bodies. Irons tend to have longer exposure ages than stones. This simply reflects their greater strength and resistance to break-up.

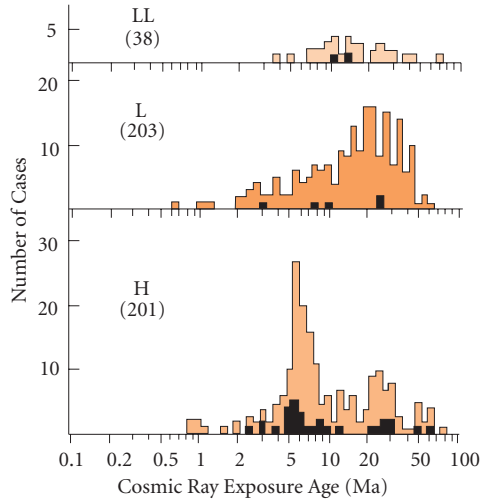

Figure 10.24 Cosmic ray exposure ages of meteorites. Filled histogram is for meteorites with regolith histories (i.e., brecciated meteorites). Crabb and Schultz (1981). With permission from Elsevier.

The limited variability in composition within meteorite classes and the compositional gaps between different classes suggest that all meteorites of a common class share a close genetic history. Relatively young cosmic ray exposure ages, the clustering of exposure ages of meteorite classes, extensive thermal metamorphism (reaching perhaps 1000°C), evidence of melting in differentiated meteorites, and slow cooling rates of iron meteorites all indicate that meteorites were once parts of larger *parent* bodies. Meteorites from a given class may have been derived from the same parent body, though this need not always be the case. Estimates of the diameters of parent bodies of various meteorite classes range from 10 to 1000 km. There are some compositional similarities between different classes that in some cases suggest a genetic relationship between them, and possible derivation from the same parent body. For example, the aubrites and e-chondrites are both highly

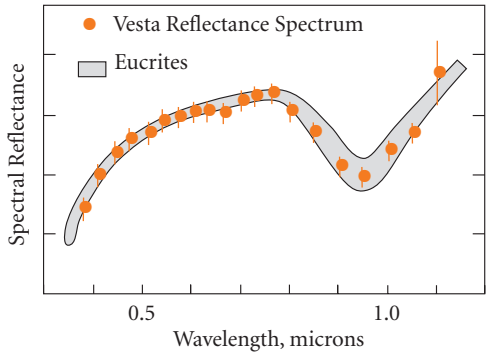

Figure 10.25 Comparison of the laboratory-determined reflectance spectrum of eucrite meteorites (basaltic achondrites) with that of the asteroid *Vesta*. The close match suggests that the crust of *Vesta* is basaltic, and similar to eucrites. McSween (1987). Reprinted with permission from Cambridge University Press.

reduced. We saw that the silicate of mesosiderites is very similar to diogenites. Many of the pallasites seem related to the IIIAB irons and may come from the same parent body. Other pallasites seem more closely related to ordinary chondrites and to IAB irons.

Orbits for a few observed falls have been reconstructed, and these reconstructed orbits confirm the suspicion that many meteorites originate in the asteroid belt. Reflectance spectra of some asteroids can be matched to specific groups of meteorites. Based on spectroscopic studies, the surface of 1 *Ceres*, the largest asteroid (diameter of 950 km), appears to compositionally match the CM chondrites. As we noted earlier, *Vesta* (Figure 10.17) has a spectrum that matches that of the eucrites (Figure 10.25) and is considered the parent of the HED achondrite group. Density and gravitational moment of *Vesta* determed by the Dawn mission indicate it has an iron core that constitutes about 18% of its mass (Russell *et al*., 2012). Radar reflections from the asteroid 16 *Psyche* suggest a Ni-Fe composition, similar to iron meteorites. The asteroid 21 *Lutetia* is thought to be similar in composition to e-chondrites based on spectral and density measurements by the European Space Agency *Rosetta* probe. S-type asteroids, which dominate the inner asteroid belt, are probably the parents of the ordinary chondrites, although this remains somewhat uncertain. Other asteroids, notably those of class "M", appear to be composed of Fe-Ni metal and are analogous to iron meteorites. It is quite interesting and important that the asteroid belt appears to be compositionally zoned, with "igneous" asteroids, analogous to the differentiated meteorites, predominating in the inner part, and "primitive" meteorites, analogous to carbonaceous chondrites, dominating in the outer part of the belt.

Although meteorites represent a wide range of compositions, there is no particular reason to believe that those in collections are representative samples of the compositions of solar system bodies. The reflectance spectra of most asteroids do not match those of any of meteorite classes – suggesting they have a greater variety of compositions than represented by meteorites. Collisions among asteroids and the gravitational influence of Jupiter probably sends a more or less constant flux of asteroid fragments into orbits that will ultimately lead to collisions with the Earth.

10.4.3 Isotopic anomalies in meteorites

10.4.3.1 Neon alphabet soup and interstellar grains in meteorites

Since Thomson's discovery that elements could consist of more than one isotope in 1912, scientists have realized that the isotopic composition of the elements might vary in the universe. They also realized that these variations, if found, might provide clues as to how the elements came into being. As the only available extraterrestrial material, meteorites were of obvious interest in this respect. However, isotopic analyses of meteorites, by Harold Urey among others, failed to reveal any differences between meteorites and terrestrial materials. This apparent isotopic homogeneity was raised as an objection to the polygenetic hypothesis of Burbidge, Burbidge, Fowler, and Hoyle (1957), since isotopic variations in space and time were an obvious prediction of this model. Within a few years of its publication, however, John Reynolds, a physicist at the University of California, Berkeley, found isotopic variations in noble gases, particularly neon and xenon (Reynolds, 1960).

Noble gases are present in meteorites at concentrations that are often as low as 1 part in 10^{10}. Though they are fairly readily isolated

and analyzed at these concentrations, their isotopic compositions are nonetheless sensitive to change due to processes such as radiogenic decay (for He, Ar, and Xe), spallation and other cosmic ray-induced nuclear processes, and solar wind implantation. In addition, mass fractionation can significantly affect the isotopic compositions of the lighter noble gases (He and Ne). Through the late 1960s, all isotopic variations in meteoritic noble gases were thought to be related to these processes. For example, Ne isotopic variations could be described as mixtures of three components, "Neon A" or planetary (similar in composition to the Earth's atmosphere), "Neon B", or solar, which differed from atmospheric due to mass fractionation, and "Neon S", or spallogenic (cosmogenic) (Figure 10.26). The isotopic variations in Xe discovered by Reynolds were nonetheless significant because they were due to the decay of ^{129}I and ^{244}Pu, which must have been only recently (on a cosmic time-scale) synthesized.

In 1969, the picture became more complex when evidence of a ^{22}Ne-rich component, named "Neon E" was found in the high-temperature (900–1100°C) release fractions of six carbonaceous chondrites (Black and Pepin, 1969). However, the carrier of Neon-E proved difficult to identify. Many scientists participated in an intensive search over nearly two decades for the carrier phase of these components. The search quickly focused on the matrix, particularly that of CM2 meteorites. But the fine-grained nature of the matrix, together with the abundance of sticky and refractory organic compounds, made work with the groundmass difficult. In the late 1980s, E. Anders and his colleagues at the University of Chicago (e.g., Tang and Anders, 1988) found that Neon-E is associated with fine-grained (<6 μm) graphite and SiC (silicon carbide) of the matrix. Ne-E actually consists of two isotopically distinct components: Ne-E(L), which was found to reside in graphite, and Ne-E(H) which resides in SiC. The ^{20}Ne/^{22}Ne ratio of Ne-E(L) is less than 0.01, while that of Ne-E(H) is less than 0.2.

The other key noble gas in this context is xenon. Having nine isotopes rather than three and with contributions from both ^{129}I decay and fission of Pu and U, isotopic variations in Xe are bound to be more complex than those of Ne. On the other hand, its high mass minimizes mass fractionation effects. Eventually, two isotopically distinct components were identified: Xe-HL, so named because it shows enrichments in both the heaviest and lightest Xe isotopes (Figure 10.27), and the Xe-S

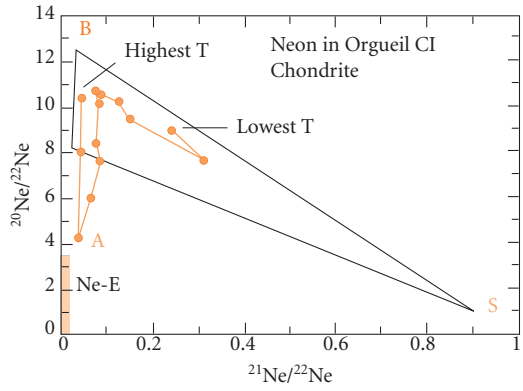

Figure 10.26 Neon isotopic compositions in a step-heating experiment on *Orgueil* CI chondrite, which produced the first evidence of "pre-solar" or exotic Ne. The points connected by the line show the changing Ne isotope ratios with increasing temperature. The shaded area is the original estimate of the composition of the pure Ne-E component. Also shown are the compositions of Ne-A ("solar"), Ne-B ("planetary"), and Ne-S ("spallogenic"). Data from Black and Pepin (1969).

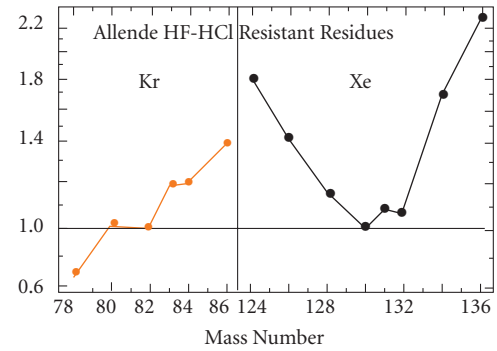

Figure 10.27 The isotopic composition of Kr and Xe of the "Xe-HL " component in *Allende* matrix. Xe-HL is characteristically enriched in both the light and heavy isotopes, while the lighter noble gases show enrichment only in the heavy isotopes. Adapted from Lewis et al. (1975).

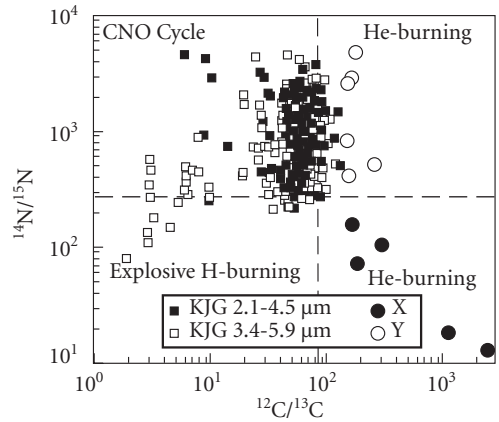

Figure 10.28 Isotopic composition of C and N in SiC from *Murchison* (CM2) meteorite. Dashed lines show the isotopic composition of normal solar system C and N. Populations X and Y, which are anomalous here, are anomalous in other respects as well. Anders and Zinner (1993). With permission from John Wiley & Sons.

component, so named because it is enriched in the s-process-only isotopes, ^{128}Xe and ^{130}Xe. Anders' University of Chicago group eventually identified the carrier of Xe-HL as microdiamonds and that of Xe-S as SiC.

Once these interstellar grains were isolated, it was possible to study their isotopic compositions in detail using ion microprobes.* Very large variations in the isotopic composition of carbon and nitrogen were found (Figure 10.28). The SiC grains do not form a single population, but represent a number of populations of grains, each produced in a different astronomical environment. Isotopic variations occur in a number of other elements, including Mg, Si, Ca, Ti, Sr, Zr, Mo, Ba, Nd, Sm, and Dy.

That the first "interstellar" or "presolar" grains discovered were unusual minerals such as graphite, SiC and diamond had to do with the way they were isolated. Essentially, they were the residues after the rest of the meteorite was dissolved away. Subsequently, however, similar isotopic anomalies have been found in Si_3N_4, spinel, hibonite, a variety of metal carbides, TiO_2, Fe-Ni metal and olivine. The latter may turn out to be the most common kind of presolar grain. In the exceptionally primitive carbonaceous chondrite *Acfer*, Nagashima *et al.* (2004) and Nguyen and Zinner (2004) found that presolar silicates were present in the groundmass at an abundance of about 30 to 40 parts per million, compared with 14 parts per million for presolar SiC.

Discovery of isotopically anomalous interstellar grains has inspired theorists to attempt to explain them, and there has been considerable progress on understanding stellar and explosive nucleosynthesis in the past two decades as a result. However, even the very limited treatment of nucleosynthetic processes in stars earlier in this chapter is sufficient to allow us to identify the environment in which some of these grains were produced. Thus, if we examine a chart of the nuclides, we quickly see that the lightest Xe isotope, ^{124}Xe, is a p-process-only nuclide, while the heaviest Xe isotopes, ^{134}Xe and ^{136}Xe, are r-process-only nuclides. The p- and r-processes occur in supernovae, thus Xe-HL, as well as perhaps the diamonds that carry it, must have been produced in supernovae. Xe-S is enriched in ^{128}Xe and ^{130}Xe, which are s-process-only isotopes. The s-process, of course, operates mainly in red giants, so we might guess the SiC was produced in red giants. Carbon and nitrogen in the SiC is, in most cases, enriched in ^{14}N and ^{13}C relative to normal solar system nitrogen and carbon. As we noted earlier in the chapter, there tends to be some net production of ^{14}N and consumption of ^{12}C in the CNO cycle, which operates in main sequence stars, but also in the H-burning shell of red giants. As it turns out, our guess of red giants as sources of this SiC would be a good one. Theoretical studies show a close match between the observed isotopic patterns and those produced in the red giant phase (also called asymptotic giant branch) of medium-sized stars (1–3 $M_\odot$). These studies show that such stars could also produce the ^{107}Pd and

* Ion microprobes fire a narrow beam of ions (often O or Cs) at a surface. This produces ions from the surface that can be analyzed in an attached magnetic sector mass spectrometer. This is known as secondary ionization mass spectrometry or SIMS. Because the ion beam can be focused very finely (a few microns in diameter), very small areas can be analyzed.

^{26}Al that was present when the meteorites formed (e.g., Wasserburg *et al.*, 1994).

10.4.3.2 Oxygen isotope variations

Another element commonly showing isotopic variations is O. Until 1973, O isotope variations in meteorites were thought to be simply the result of mass-dependent fractionation, as they are on Earth. But when R. Clayton of the University of Chicago went to the trouble of measuring ^{17}O (0.037% of O) as well as ^{18}O and ^{16}O, he found that these variations were not consistent with simple mass-dependent fractionation. This is illustrated in Figure 10.29. On a plot of ^{17}O/^{16}O versus ^{18}O/^{16}O, almost all terrestrial materials (atmospheric ozone is a notable exception, as we learned in Chapter 9) plot on a line with a slope of 0.52 – the *terrestrial fractionation line*. Lunar samples fall on this same line, but meteorites and meteoritic components do not, and some appear to plot on a line with a slope of 1. The initial interpretation was that this reflected mixing between a more or less pure ^{16}O component, such as might be created by helium

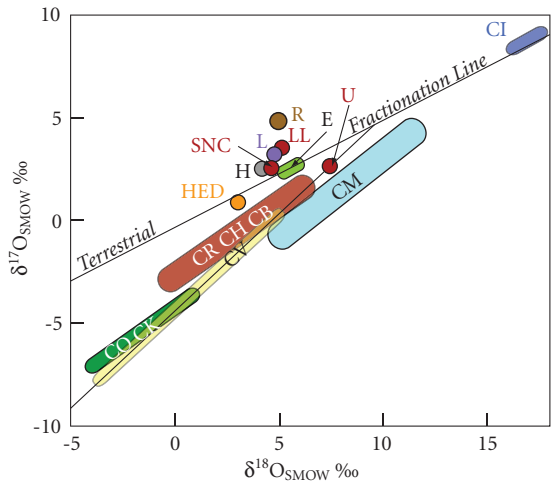

Figure 10.29 Variation of O isotope ratios in meteorites: CO, CK, etc., carbonaceous chondrites; H, L, LL, ordinary chondrites; HED, howardites, eucrites, diogenites; U, ureilites; SNC, Shergottiites, naklites, Chausigny; E: enstatite chondrites. The Earth, Moon, and aubrites have the same isotopic composition as enstatite chondrites. Modified from Clayton (1993). Reproduced with permission.

burning, injected into the solar nebula by a red giant, and a component of "normal" isotopic composition. A decade later, experiments conducted by Thiemens and Heidenreich (1983) suggested a different interpretation. They found that ozone produced by a high-frequency electrical discharge showed "mass-independent fractionation", where the ozone was equally enriched in ^{17}O and ^{18}O relative to ^{16}O. The experiment demonstrates that a slope of 1 on the δ^{17}O–δ^{18}O diagram could be produced by chemical processes. Thiemens suggested this kind of fractionation arises because non-symmetric (e.g., ^{16}O^{17}O or ^{18}O^{16}O) molecules have more available energy levels than symmetric (e.g., ^{16}O^{16}O) molecules (as we saw in Chapter 9, symmetry enters into the calculation of the partition function). Since then, mass-independent fractionation has been found in ozone of the Earth's atmosphere as well as in Archean sulfides and sulfates, so there is no question that it can occur in nature.

A somewhat different idea was proposed by Clayton (2002). He suggested that the anomalies arose through radiation self-shielding in the solar nebula. In his model, ultraviolet radiation from the early protosun dissociated carbon monoxide, which would have been among the most abundant gases in the solar nebula. Because C^{16}O rather than C^{17}O or C^{18}O was the dominant oxygen-bearing species, the radiation of the wavelength necessary to dissociate C^{16}O would have been quickly absorbed as it traveled outward from the Sun. At greater distance from the Sun, radiation of the frequency necessary to dissociate C^{16}O would have been absent, while that needed to dissociate C^{17}O and C^{18}O would still be available. Thus at these distances, C^{17}O and C^{18}O are preferentially dissociated, and equally so, making ^{17}O and ^{18}O preferentially available for reaction to form silicates and other meteorite components. Since the solar nebula would have been fairly opaque at this time, this isotopic fractionation would have occurred in the inner part of the nebula, near the forming star, and then expelled back out by the "X-wind". The implication of this is that most of the solid matter that makes up the Earth and it neighbors must have cycled through this inner region at one point. Clayton's model also predicts that the Sun itself should be poor in ^{18}O

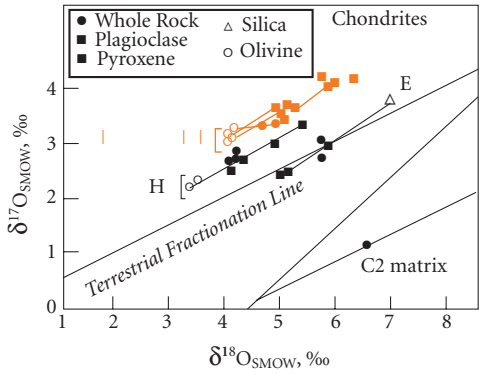

Figure 10.30 O isotope variation among minerals of various meteorite classes (Clayton *et al.*, 1976). With permission from Elsevier.

and ^{17}O compared with meteorites and the Earth – closer in composition to the CAIs. This prediction appears to have been recently confirmed based on analysis of solar wind implanted in lunar soil.

As Figure 10.30 shows, while variations *between* classes are mostly mass-independent, variations *within* groups of meteorites fall along mass-dependent fractionation lines. This strongly suggests that, for the most part, different groups could not have come from the same parent body and that the different groups probably formed in different parts of the presolar nebula. There are a few exceptions: IIE irons fall on a mass-dependent fractionation line (MDFL) with H-chondrites, IVA irons plot on a MDFL with L and LL chondrites, and basaltic and hypersthene achondrites plot on a MDFL with IAB irons and some stony-irons. This suggests a genetic relationship between these objects, perhaps derivation from a single parent body. The Moon and the Earth plot on a single MDFL, evidence of their close genetic relationship. Intriguingly, the enstatite chondrites also plot along the terrestrial fractionation line. This has led some to suggest that enstatite chondrites might be a better compositional model for the Earth than either carbonaceous or ordinary chondrites.

10.5 ASTRONOMICAL AND THEORETICAL CONSTRAINTS ON SOLAR SYSTEM FORMATION

As the preceding sections show, meteorites provide some tremendous insights into the formation of our solar system. However, before we try to use these observations to draw some conclusions about how the solar system, and the Earth, formed, we need to consider several other sets of observations. The first of these is astronomical observations of star formation occurring elsewhere in the universe. As it turns out, star formation is more or less an everyday event in the universe and we can watch it happening. The second is theoretical considerations of how solids condense from a hot gas of solar composition. We have seen that meteorites provide evidence for at least transient high temperatures in the early solar system. What can we expect when hot gas cools? We can use thermodynamics to find the answer. Finally, any theory of solar system formation must successfully predict the solar system as it exists. Consequently, we'll briefly review the nature of our solar system.

10.5.1 Evolution of young stellar objects

Astronomical observations have established that stars form when fragments of large molecular clouds collapse, as is occurring in the Great Nebula in Orion (Figure 10.31). Such clouds may have dimensions in excess of 10^6 AU* and masses greater than $10^6 M_O$ (solar masses). Typically, about 1% of the mass of these clouds consists of submicron-sized dust, about 1% is gaseous molecules heavier than He, and the remainder is H_2 and He gas. Gravity will tend to make such clouds collapse upon themselves. This tendency may be resisted by thermal motion that tends to expand the cloud, rotational motion that stabilizes it against collapse, and internal pressures generated by turbulence. More recent observations reveal that magnetic fields, which couple to the ionized fraction of the gas, play a key role in stabilizing these clouds. A careful balance between the forces tending to collapse the cloud and forces tending to

* AU stands for Astronomical Unit, which is the Earth–Sun distance or 1.49×10^8 km.

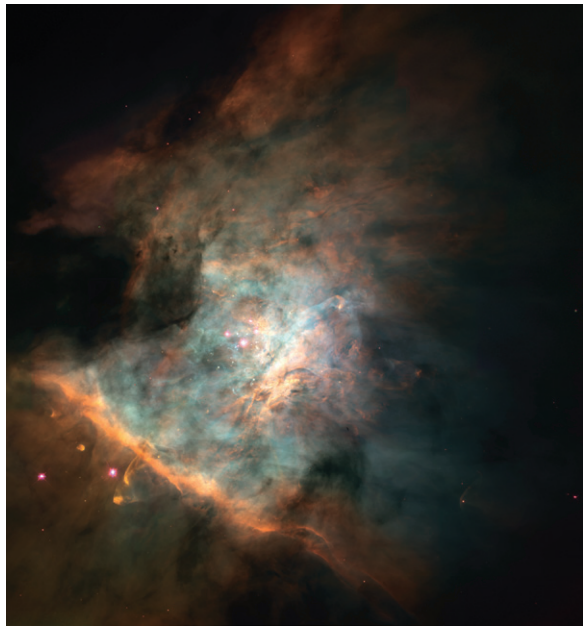

Figure 10.31 The Great Nebula in Orion, shown in a Hubble Space Telescope photograph, is a cloud of gas and dust within which stars are forming. Image: NASA.

expand it can result in the cloud being stable indefinitely. Collapse of a part of a nebula can occur through the removal of a supporting force, magnetic fields in particular, or by an increase in an external force, such as a passing shock wave.

In addition to random density perturbations that can spontaneously collapse, shock waves could trigger cloud collapse and star formation. One potential source of shock is supernovae. Another is the density waves that manifest themselves as the spiral arms of the galaxies. We can think of the galactic arms as being similar to a traffic jam on the galactic orbital freeway. Though traffic continues to flow through the region of the traffic jam, there is nevertheless a sort of self-perpetuating high concentration of stars in the traffic jam itself. As clouds are pulled into the arms, they are compressed by collisions with other matter in the arms, leading to collapse of the clouds and initiation of star formation.

The Taurus-Auriga cloud complex is a good example of a region in which low-mass stars similar to the Sun are currently forming. The cloud is about 6×10^5 AU across, has a mass of roughly $10^4\,M_\odot$, a density of 10^2–10^3 atoms/cm^3, and a temperature around 10 K. Embedded within the cloud are clumps of gas and dust with densities two orders of magnitude higher than the surrounding cloud. Within some of these clumps are luminous protostars. About 100 stars with mass in the range of 0.2–3 $M_\odot$ have been formed in this cloud in the past few million years.

As the cloud collapses, it will warm adiabatically, resulting in thermal pressure that opposes collapse. Magnetic fields inherited from the larger nebula will intensify as the system contracts, and can accelerate charged particles away from the forming star. Further intensification of the magnetic field occurs as an increasing fraction of the material ionizes as temperature increases. Finally, even small amounts of net angular momentum inherited from the larger nebula will cause the system to spin at an increasing rate as it contracts. For a cloud to collapse and create an isolated star, it must rid itself of over 99% of its angular momentum in the process of collapse. Otherwise the resulting centrifugal force will break up the star before it can form. Much of what occurs during early stellar evolution reflects the interplay between these factors.

Protostellar evolution of moderate-sized stars (i.e. stars similar to the Sun) can be divided into 5 phases, labeled –I, 0, I, II, and III, based on the spectra of their electromagnetic emission (Lada and Shu, 1990; Boss, 2005a). The first phase, the –I phase, is the initial collapse of a molecular cloud to form a protostellar core and nebular disk. No astronomical examples of this phase have been found, so understanding this phase depends entirely on theoretical calculations. Model calculations show that once a cloud fragment or clump becomes unstable, supersonic inward motion develops and proceeds rapidly as long as the cloud remains transparent and the energy released by gravitational collapse can be radiated away. Once the cloud becomes optically dense so that energy is no longer radiated away, the collapse slows. At this point, the protostellar core has a radius of about 10 AU and a mass of perhaps only 1% of the final mass of the star. When tem-

peratures in the core reach 2000 K, energy is consumed in the dissociation of hydrogen, allowing further collapse and bringing the radius down to several times that of the eventual star. For a star of about 1 solar mass, the time-scale is thought to be roughly 10^6 to 10^7 years. It is longer for smaller stars and shorter for larger ones.

For subsequent phases, observations at wavelengths ranging from radio waves to X-rays provide a wealth of information on protostellar objects and their nebulae. During phase 0, the protostar is deeply embedded in its surrounding cocoon of gas and dust and cannot be directly observed. At the beginning of the phase, the mass of the protostellar core is still very much smaller than that of the infalling envelope of gas and dust. In the meantime, angular momentum progressively flattens the envelope into a rotating disk, the stellar nebula. Material from the surrounding envelope continues to accrete to the disk, but mass is also transferred from the disk to the protostellar core at a slow rate.

The object L1551 IRS5 in the constellation Taurus is considered the prototypical Class I object, and detailed observations of it over the last decade have provided considerable insights into this stage of stellar evolution. Observations at radio wavelengths revealed there are actually two protostars about 45 AU apart with a combined mass of about 1 M_O (binary stars are more common that individual stars such as the Sun). The protostars are deeply embedded in circumstellar disks that have diameters of about 20 AU. Because they are optically thick, temperatures in the interior of these disks cannot be determined directly. However, surface temperatures of the disks can be determined from the infrared spectra of these objects and they range from 50 to 400 K at 1 AU and drop off exponentially with distance. Models that reproduce these surface temperatures have disk interior temperatures that range from 200 to 1500 K at 1 AU and decrease exponentially with radial distance. The highest temperatures, which are enough to vaporize silicates, are likely short-lived and persist only for a period of perhaps 10^5 yr during which accretion rates are highest. More moderate temperatures, in the range of 200–700 K, could persist in the inner part of the disk for substantially longer than this.

A very interesting feature of L1551 IRS5 and other Class I objects is strong "bipolar flows" or jets oriented perpendicular to the circumstellar disks that extend some 1000 AU from the disks. The jets consist of gas moving outwards at velocities of 200–400 km/sec. Within these jets, temperatures may locally reach 100,000 K. As the material in the jets collides with the interstellar medium it creates a shock wave that in turn generate X-rays. The physics that generates these jets is incompletely understood, but magnetic fields undoubtedly play a dominant role. In one theory, the X-wind model (Shu *et al.*, 1997; Shang *et al.*, 2000), the bipolar outflows are the cores of a much broader outflow that emerges from the innermost part of the circumstellar disk as it interacts with the strong magnetic field of the central protostar. As Shang *et al.* (2000) wrote, "in the X-wind model, the combination of strong magnetic fields and rapid rotation of the young star-disk system acts as an 'eggbeater' to whip out part of the material from the surrounding disk while allowing the rest to sink deeper in the bowl of the gravitational potential well". The jets and associated X-wind remove both mass and angular momentum from the system (Figure 10.32). The latter is particularly important, because as material is accreted from the disk to the star, conservation of angular momentum causes the star to rotate ever faster. Shang *et al.* (2000) estimated that about a third of the mass accreted to the disk and a larger fraction of the angular momentum is carried away by the X-wind. If this angular momentum were not lost in some way, the resulting centrifugal force would break up the star.

Phase II is represented by so-called *classical T-Tauri stars*, of which the star T-Tauri (now known to be a binary pair) is the type example. During this phase, a visible star begins to emerge from its cocoon of gas and dust, but it remains surrounded by its circumstellar disk (Figure 10.33). The star has a cool surface (4000 K) but luminosity several times greater than mature stars of similar mass (Figure 10.1). The luminosity is due entirely to continued accretion and gravitational collapse – fusion has not yet ignited in its interior. A T-Tauri star of one solar mass would have a diameter still several times that of the Sun. X-ray bursts from these stars suggest a more

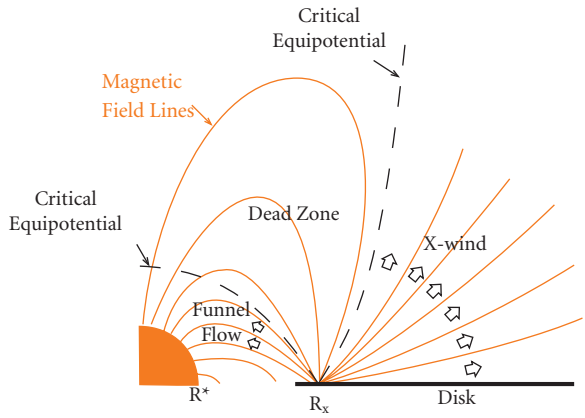

Figure 10.32 Cartoon illustrating the X-wind model. As a result of interaction with the accretion disk, the magnetic field lines of the young star truncate at radius R_x, which typically has a value of a few stellar radii. For disk material in stable orbit at R_x, two equipotential surfaces emerge from the disk, such that gravity dominates inward of the inner one and centrifugal force dominates outward of the outer one. Between these surfaces is a "dead zone" into which matter cannot freely flow. Thus matter swept off the disk surface by magnetic forces will either be pulled into the star in "funnel flow" or move away from the star as the "X-wind". Adapted from Shang *et al.* (2000).

active surface than that of mature stars, likely driven by strong stellar magnetic fields and their interaction with the accretion disk. The surrounding disk is still warm enough to give off measurable IR radiation.

Accretion to the star continues in this phase, but has dropped to rates of 10^{-6} to $10^{-8}\,M_\odot$ per year. The accretion continues to drive bipolar outflows and associated X-wind (Figure 10.32). Typical mass loss rates from the flows and winds are $10^{-8}\,M_\odot$ per year. These winds may be important for a number of reasons. First, the mass loss is significant compared with the inferred accretion and infall rates, meaning there may be little or no net accretion. Second, the outwardly blowing gas has the potential to fling solids outward to the cooler, more distant parts of the disk. In the process, solids are lifted above the disk close to the star where they are exposed to the intense radiation and are heated in the process.

Both Class I and II objects can go through occasional "FU Orionis outbursts". The name FU Orionis derives from a star in the Orion nebula that suddenly brightened by six magnitudes over 6 months in 1936. Its luminosity has been slowly decaying since then. During such an outburst, the disk outshines the central star by factors of 100–1000, and a powerful wind emerges, producing mass losses of $10^{-6}\,M_\odot$ per year in the case of FU

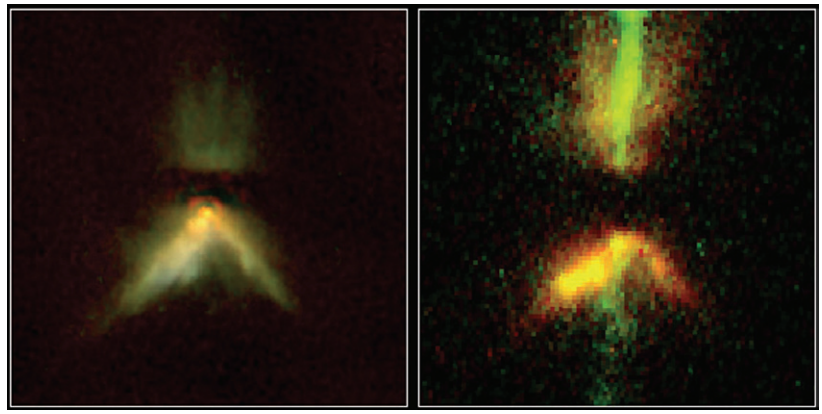

Figure 10.33 Two Hubble Space Telescope views of the T-Tauri star DG Tau B. The image on the left is taken with the Near Infrared Camera and Multi-Object Spectrometer, and the image on the right is taken with the Wide Field Planetary Camera. The accretion disk is a dark horizontal band in both images. The bipolar outflows appear green in the visible image. Infrared interferometry indicates there is a gap of about 0.25 AU between the star and the inner edge of the disk, which extends out about 100 AU. Image: NASA.